Synchrotron X-ray Reflectivity Studies on Nanoporous Low Dielectric Constant Organosilicate Thin Films[†]

Weontae Oh,[*] Yeong Do Park,[‡] Yongtaek Hwang,[§] and Moonhor Ree[§]

Department of NanoTechnology, Dong-eui University, Busan 614-714, Korea. [*]E-mail: wtoh2005@deu.ac.kr
[‡]Department of Advanced Materials Engineering, Dong-eui University, Busan 614-714, Korea
[§]Department of Chemistry, National Research Laboratory for Polymer Synthesis & Physics, Center for Integrated Molecular Systems, and BK School of Molecular Science, POSTECH, Pohang 790-784, Korea
Received October 22, 2007

Spatially resolved, quantitative, non-destructive analysis using synchrotron x-ray reflectivity (XR) with subnano-scale resolution was successfully performed on the nanoporous organosilicate thin films for low dielectric applications. The structural information of porous thin films, which were prepared with polymethylsilsesquioxane and thermally labile 4-armed, star-shaped poly(ε-caprolactone) (PCL) composites, were characterized in terms of the laterally averaged electron density profile along with a film thickness as well as a total thickness. The thermal process used in this work caused to efficiently undergo sacrificial thermal degradation, generating closed nanopores in the film. The resultant nanoporous films became homogeneous, well-defined structure with a thin skin layer and low surface roughness. The average electron density of the calcined film reduced with increase of the initial porogen loading, and finally leaded to corresponding porosity ranged from 0 to 22.8% over the porogen loading range of 0-30 wt%. In addition to XR analysis, the surface and the inner structures of films are investigated and discussed with atomic force and scanning electron microscopy images.

Key Words : Nanoporous organosilicate, Thin film, Low-k, X-ray reflectivity

Introduction

Porous organosilicate thin films have recently attracted much interest due to their potential applications as ultra low dielectric interlayers,[1-4] chemical and biosensor membranes,[5,6] catalyst hosts,[7,8] and gas separation membranes.[9] Well-known method for preparing porous organosilicates is the templated sol-gel synthesis of organosilanes.[10-14] Incorporating the nanometer-sized, air-filled pores in the interlayered matrix film is one possible and effective method for reducing dielectric constant. In order to obtain the uniform distribution of nano-sized pores in a polymer matrix, star-shaped poly(e-caprolactone) (PCL) as an organic porogen template is widely applied with poly(methylsilsesquioxane) (PMSSQ) as a polymer matrix.[12,13] The pores in an organosilicate matrix are derived by sacrificial thermal degradation of the porogens at 250-350 °C. Moreover, the thermal curing of PMSSQ precursors actively proceeds in the same temperature range (250-350 °C). The critical issues on making nanopores in a matrix film are the porogen aggregation and the generation of percolated pores, which make the film unsuitable for use in advanced ICs with small feature sizes.[1] To minimize the porogen aggregation in a polymer matrix, the hydroxyl end groups of PCL were functionalized to reactive triethoxysilyl groups as described elsewhere.[2-4] The chemical modification of PCL end groups aimed to bond chemically the PCL porogens with PMSSQ and restrict the phase separation of both PMSSQ matrix and PCL components. Due to the similarity of these reactive functional groups, porogens are more miscible with PMSSQ precursors and lead to the significant reduction of aggregation in these composite films. The ability to characterize the structure of a porous film such as pore structure and distribution within the film is as important as developing the dielectrics and porogens themselves.

In this study, we quantitatively investigated structures, surface roughnesses, and laterally averaged electron densities of porous organosilicate thin films using synchrotron X-ray reflectivity. The nanoporous organosilicate thin films were prepared with soluble PMSSQ precursor containing reactive ethoxysilyl and hydroxysilyl groups as a dielectric matrix material and 4-armed, star-shaped poly(ε-caprolactone) (PCL) as an organic porogen. In specular x-ray reflectivity (XR), a part of incident beam above a critical angle ($\theta_{c,film}$) penetrates into a film and reflects from the interface between film and substrate. This makes the uniform oscillation frequency of an intensity profile as the waveguide mode for x-rays confined in the film. The detailed structural information about a thin film is extracted from the characteristic XR profiles.[12,15] The electron density and the total thickness of a thin film are directly related to the uniform oscillations, the critical angle, and the decaying mode of the profile. The XR gives the precise structural information of a thin film in terms of the laterally averaged electron density profile along the film surface normal. In addition, we compared these results with our previous works,[21] which were studied with PMSSQ and 6-armed PCL analogs.

[†]This paper is dedicated to Professor Sang Chul Shim (Kyungpook National University) in the honor of his retirement.

Experimental

The synthesis of PCL porogens and their reactive end modification with triethoxysilyl groups were conducted as described elsewhere;[2,3,16] A four-armed PCLs ($\overline{M}_w$ = 6,800, polydispersity index (PDI) = 1.10, and an average degree of polymerization per arm = 8.9) were synthesized by the ring-opening polymerization of ε-caprolactone with di(trimethylol propane) as a four-armed core material, according to the method by Shin *et al.*.[16] Hydroxyl end groups of the as-synthesized PCLs were further chemically modified by reaction with 3-isocyanatopropyltriethoxysilane, finally to produce triethoxysilyl-terminated PCL molecules noted as mPCLs (see Figure 1). PCL and its triethoxysilyl analogue are well known as thermally labile porogens. A soluble PMSSQ precursors ($\overline{M}_w$ = 10,000) containing ethoxysilyl and hydroxysilyl groups were supplied by Techneglas Company (Perrysburg, OH, USA). The PMSSQ precursors undergo curing reaction over the temperature region 75-340 °C by thermal condensation, and the cured PMSSQs are stable up to 500 °C.[3] Because the thermal curing condition of triethoxysilyl-terminated PCL (mPCL) is overlapped with PMSSQ precursor, the chemical hybridization of PMSSQ and mPCL is likely to occur in their blends and the aggregation of mPCL molecules can be minimized prior to the sacrificial thermal decomposition. For comparison, the unmodified, hydroxyl-terminated four-armed PCLs were applied to prepare the porous PMSSQ thin films.

Thin films of PMSSQ/porogen composites were prepared in methyl isobutyl ketone (MIBK) solutions with a various compositions of PMSSQ precursors and porogens, in which each solution was filtered using a PTFE-membrane micro-filter of pore size 0.20 mm, spin-coated onto the precleaned Si(100) substrates at 3000 rpm for 30 s and subsequently dried at 50 °C for 60 min in N_2 atmosphere. The dried thin films were heated up to 200 °C at a rate 2 °C/min and thermally cured at that temperature for 100 min. In order to prepare porous thin films, the cured thin films were further heated up to 400 °C at a rate 2 °C/min and the organic porogens (mPCLs) in the composite thin films were thermally decomposed at that temperature for 60 min. The whole thermal process was conducted under vacuum. The thermal treatment conditions in this work were adapted from the previous thermal studies of PMSSQ and PCL organic porogens.[3,17] The thickness of a resulting thin film was *ca.* 90 nm, as determined by ellipsometry.

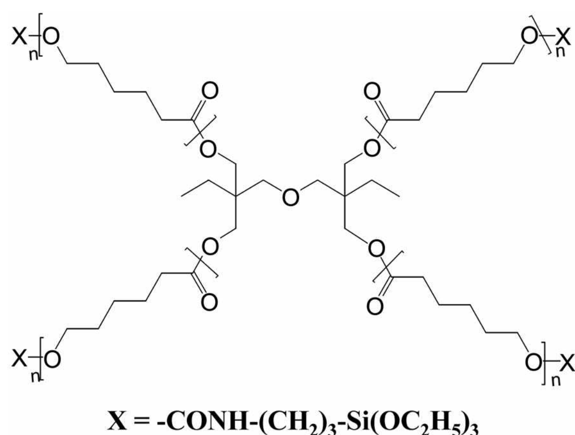

Figure 1. Chemical Structures of thermally-labile four-armed poly(ε-caprolactone) (mPCL).

Specular X-ray reflectivity (XR) data were collected using synchrotron radiation at a bending magnet x-ray scattering beamline BL3C2 of the Pohang Accelerator Laboratory. The x-ray radiation was selected to be a wavelength λ of 1.54 Å in an energy resolution of $\Delta\lambda/\lambda = 5 \times 10^{-4}$ and a scintillation counter with an enhanced dynamic range (Bede Scientific, EDR) was used as a detector. The measured intensity of the reflected x-rays, which were collected in a specular direction by a θ-2θ scanning, was normalized to that of primary X-rays monitored by an ionization chamber. A sample alignment was specially taken care for precision as described by Gibaud *et al.*.[18] The measured XR data were quantitatively analyzed with a recursive formula given by the dynamic theory of Parratt.[15] The pore distribution along with film thickness in porous PMSSQ thin film was characterized by field emission scanning electron microscopy (FE SEM, Hitachi S-4200, operated at 5 kV). In addition, the surfaces of porous thin films were investigated by atomic force microscopy (AFM, Park Scientific Instruments, Autoprobe AP-100).

Results and Discussion

The PMSSQ precursors undergo the evaporation of the water and ethanol byproducts by thermal curing in the temperature range 75-350 °C. Triethoxysilyl-terminated PCLs (mPCLs) also have the similar thermal curing window with PMSSQ precursors because they have the same hydroxyl and ethoxysilyl end groups. This concurrence of the curing reactions of the porogen and precursor components is attributed to the chemical hybridization of the components, which prevents the formation of large porogen aggregates. Based on this thermal behavior of precursors and porogens, we prepared the porous PMSSQ dielectric flms imprinted with mPCL porogens in a vacuum by thermal treatment up to 400 °C.

In order to analyze the structures of thin film surfaces and interfaces, x-ray reflectivity can be applied in the field of nanoporous films for low dielectrics.[12,15,21] The critical angle ($\theta_c = \lambda(\rho_e r_e/\pi)^{1/2}$) is directly related to the average electron density in a film, and the total thickness of a film is extracted from the oscillation frequency of a uniform mode. Figure 2 shows the representative experimental XR curve with the best model fit assuming a homogeneous electron density distribution within a film, which was prepared with a solution in MIBK (solid content of 5 wt.%) of PMSSQ/mPCL (90/10 w/w) and calcined at 400 °C to thermally decompose and eliminate the mPCL porogens in the film. The two critical angles from a film ($\theta_{c,film}$) and a substrate ($\theta_{c,Si}$) were clearly identified around the glazing incident angles θ smaller than 0.35 nm^{-1}. The decay mode of XR

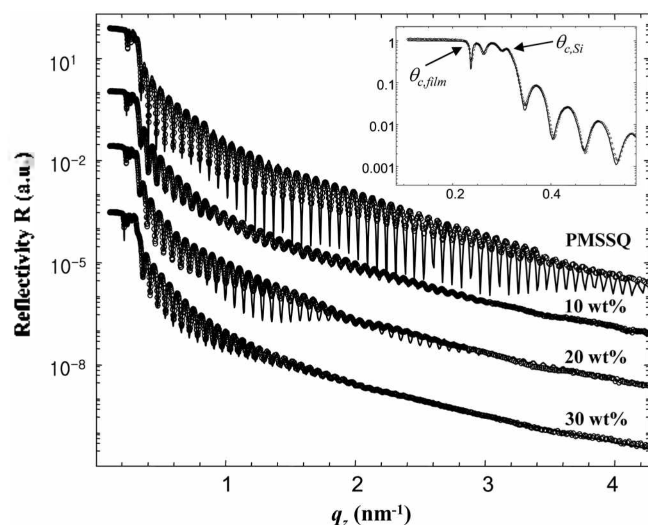

Figure 2. X-ray reflectivity curves and best fits of porous PMSSQ films, which was prepared with various mPCL loadings and calcined at 400 °C to completely remove mPCLs. The precents in this figure represent the initial porogen contents; Experimental XR data (closed circle symbols) and best fit curve (solid line). The inset enlarged from the initial loading of 10 wt% shows the critical angles of film (θ_c, *film*) and Si substrate (θ_c, *Si*).

curve with high frequency oscillations is mainly caused by the roughness of a surface and an interface. The high frequency oscillations, commonly called as Kiessig fringes,[19] are due to interference between the beams reflected from the film/air and the film/substrate interfaces. The experimental data were well matched with the fitted curve (solid line in Figure 2), which was obtained on the assumption of homogeneous distribution of electron density along the thickness direction except for a thin skin layer; the film has an average thickness of 85.3 nm and an average electron density of 364 nm^{-3}.

The fit parameters of experimental XR data on porous PMSSQ films were summarized in Table 1. We found that porous PMSSQ films imprinted with 0-20 wt% initial porogen loadings had skin layers on the inner bulk layer. According to the previous result[12] the skin layer was explained by the cooling process of the cured films, which proceeds from the film surface in the direction of the substrate, and proved by the broad and low frequency modulations in the whole XR curve. The phase of this modulation unambiguously indicates that the electron density of the skin layer is slightly different from that of the underlying bulk layer. The electron densities of the porous PMSSQ films were higher than the inner bulk layers. However, the broad and low frequency modulations were not found in XR curve of Figure 2, and the skin layers of porous PMSSQ films (from the initial porogen loadings of 10 and 20 wt%) showed lower electron densities than inner bulk layers of the films unlike the previous result. Moreover, the porous film imprinted with a 30 wt% porogen loading revealed to have no skin layer. These changes of ρ_e(skin) on porous PMSSQ films supports that the formation of PMSSQ film might be significantly influenced by sacrificial thermal degradation process of the porogen molecules, although the crosslinking reaction of the PMSSQ precursors favors at the PMSSQ-air interface than in the bulk film. The sacrificial thermal degradation of the porogens in a PMSSQ composite film mainly proceeds by out-gassing toward the film surface and the out-gassing of the decomposed byproducts make the skin layer rough. Therefore, no observation of skin layer in a porous film imprinted with a 30 wt% porogen loading indicates that the excessive out-gases by the initially-loaded porogens have destructed the skin layer. The film surface roughness determined from XR curve fitting was in the

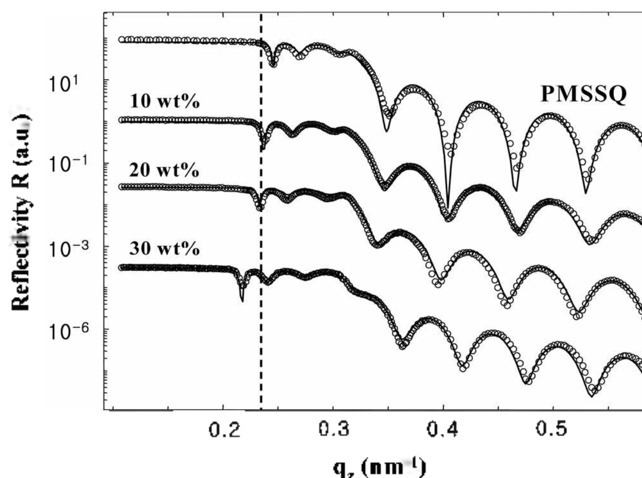

Figure 3. Experimental and fit curves of x-ray reflectivity around two critical angles of porous PMSSQ films after calcination at 400 °C. The symbols and the solid lines represent the experimental data and the fits, respectively; the solid contents of mPCL templates in original composite films were (a) 0 wt%, (b) 10 wt%, (c) 20 wt%, and (d) 30 wt%.

Table 1. Best fit parametes of experimental XR data on nanoporous PMSSQ films

Templates (wt%)	Thickness (nm)^a		σ^b (nm)	Electron Density (nm^{-3})^c			P_{ref}^d (vol%)
	d (IL)	d (SL)		ρ_e (IL)	ρ_e (SL)	$\rho_{e,av}$ (film)	
0	81.1	4.9	0.6	396	443	399	–
10	82.3	3.0	0.8	366	301	364	8.8
20	82.1	4.8	0.9	355	280	351	12.0
30	95.7	–	1.2	308	–	308	22.8

^{a}Thickness of bulk and skin layers. The uncertainty for the total film thickness is ±0.1 nm. ^{b}Film surface roughness by XR analysis. ^{c}Electron densities of the bulk and the skin layer, and averaged over the entire film. The uncertainty for $\rho_{e,av}$ is ±5 nm^{-3}. ^{d}Porosity estimated with respect to the PMSSQ film.

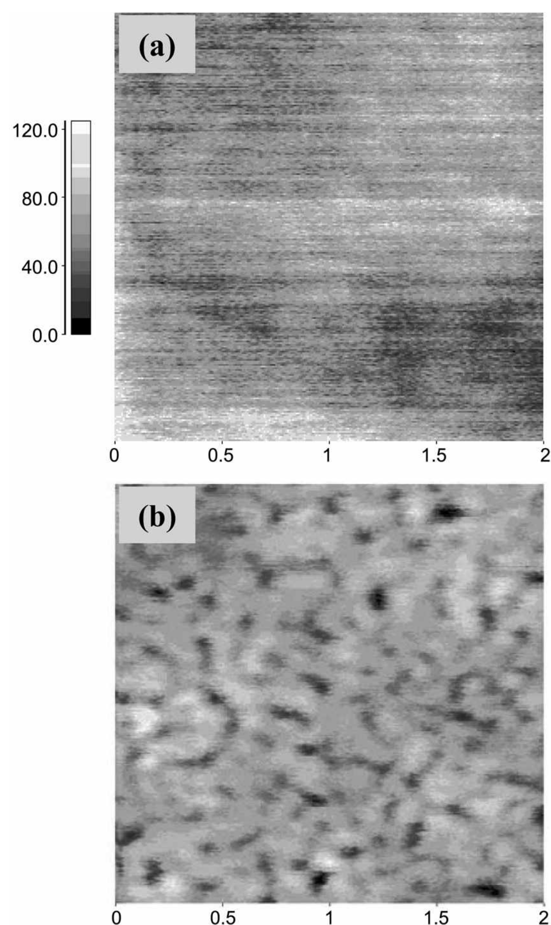

Figure 4. AFM images of porous PMSSQ films imprinted with mPCLs of (a) 20 wt% and (b) 30 wt%.

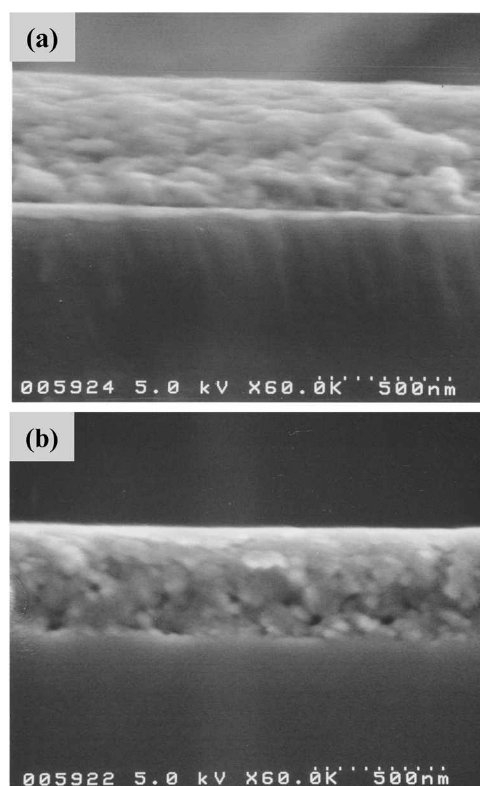

Figure 5. FE SEM images of porous PMSSQ films prepared from (a) PMSSQ/mPCL (70/30 w/w) and (b) PMSSQ/PCL (70/30 w/w).

range of 0.6-1.2 nm over the porogen loading range of 0-30 wt%, which were similar to rms roughness (0.5-1.4 nm) determined by AFM (see Figure 4). Compared to the previous results[21] which were studied with PMSSQ and 6-armed PCL analogs, the nanoporous PMSSQ thin films imprinted with 4-armed PCLs showed the lower roughness and porosities. These characteristics of the nanoporous thin films are caused by the structure differences of 4-armed PCL with the lower numbered branches and reactive end groups.

Figure 3 shows the experimental XR profiles around the critical angles of the porous films imprinted with various porogen loadings, along with the fitted curves. The XR analysis was based on the assumption of homogeneous electron density distribution throughout the film except for a thin surface skin layer with thickness of *ca.* 4 nm. This figure also shows that the critical angle of a calcined film shifts to the lower q_z region by the complete decomposition and elimination of mPCL porogens at thermal treatment up to 400 °C as the initial porogen loading increases from 0 to 30 wt%. It indicates that a well-defined porous structure was developed in a film with mPCL loading during the above thermal treatment. All of fitting parameters were precisely determined from the experimental data which were well matched with the corresponding fits (see Table 1). The lower critical angle implies the lower electron density of the corresponding film, which supports higher porosity in the resulting film. We have already mentioned from the previous works[2-4] that triethoxysilyl groups of mPCL porogen molecules restrict their mobility in the PMSSQ composite film due to chemical bonding with PMSSQ, and nano-sized pores in its calcined film are generated by the decomposition and elimination of the thermally labile mPCLs in the homogenous composite film during thermal process.[2,3] The porosity (P_{rel}) of Table 1 corresponds to the relative porosity with respect to the electron density, $\rho_{e,av}(film)$ of the PMSSQ dielectric thin film. The estimated P_{rel} value increases from 8.8 to 22.8% as the initial porogen loading increases from 10 to 30 wt%.

In addition, AFM surface images (Figure 4) show that the higher porogen loading leads to the worse surface roughness. On the porogen loading of 30 wt%, the surface region of the lower electron density should be considered as a rough interface between air and film, not a skin layer. In order to compare the pore distributions along with film thickness, we prepared another porous film imprinted with the unmodified porogen (PCL), and took both cross-sectioned SEM images, which showed the pore distributions along with film thickness. The electron densities of porous films imprinted with PCLs exhibited similar trend with those of porous films from mPCL/PMSSQ composites, but the inner pore distribution of the porous film imprinted with PCLs were apparently different from that of the porous film imprinted with mPCLs. The cross-sectioned SEM images of Figure 5 showed the disparity of the inner pore distributions

of the porous films; the film imprinted with PCLs showed the submicro-sized pores, which were heterogeneously distributed along with the film thickness. However, there was no visible-sized pore in the film imprinted with mPCLs and its sectional image was very smooth. We have also found the closed, spherical pores with size of *ca.* 5 nm from TEM image (see the TEM image of ref. 20). This shows that mPCLs randomly dispersed within the PMSSQ composite film have successfully generated well-controlled nanopores in the dielectric film.

Taking the SEM and TEM results into account, it is proved that the triethoxysilyl-modification of PCL porogen is very effective on nano-sized pore generation in PMSSQ film. The theoretical and quantitative XR analysis on a thin film has presented more significant information about a thin film structure, as combined with other techniques such as TEM or SEM imaging. Compared to unmodified PCL porogen, the loadings of mPCL in PMSSQ have given better effect on making a low dielectric nanoporous thin film. This is mainly due to the superior resistance of mPCL against pore collapse under thermal process of composite films. The higher number of reactive end groups leads to the thicker networked walls around their surroundings. Therefore, the pores imprinted with mPCLs are more stable and less aggregated than those imprinted with PCLs.

Conclusions

XR studies were performed on PMSSQ dielectric thin films imprinted with unmodified and reactive triethoxysilyl-modified PCL porogens. The PMSSQ/porogen thin films prepared in various compositions were thermally treated to cure the composite films and subsequently decompose the porogens in the films. The detailed structural information of porous thin films was investigated by quantitative, non-destructive XR and AFM analysis as well as destructive SEM. The presence of top skin layer was identified by the different electron density from the underlying bulk layer of a film. This is inferred to be caused by the inhomogeneity of porogens or pores as well as the surface-favorable crosslinking process of the cured film. Thin skin layers of lower electron densities were distinguished in the films imprinted with porogen loadings of 0-20 wt%, but the film imprinted with a 30 wt% porogen loading did not have a skin layer. XR analysis showed that the relative porosities of porous films ranged from 0 to 22.8 as increasing the initial porogen loading from 0 to 30 wt%. The cross-sectioned SEM images supported that the reactive end group functionalization of porogens apparently improved the homogeneity of nanopore distribution and generated the well-defined nanopore structures.

Acknowledgment. This work was supported by Dong-eui University Grant (2006AA173). Synchrotron XR measurements at the Pohang Accelerator Laboratory were supported by the Ministry of Science & Technology and the POSCO company.

References

1. Ree, M.; Yoon, J.; Heo, K. *J. Mater. Chem.* **2006**, *16*, 685.
2. Lee, B.; Oh, W.; Yoon, J.; Hwang, Y.; Kim, J.; Landes, B. G.; Quintana, J. P.; Ree, M. *Macromolecules* **2006**, *38*, 8991.
3. Lee, B.; Oh, W.; Hwang, Y.; Park, Y.-H.; Yoon, J.; Jin, K. S.; Heo, K.; Kim, J.; Kim, K. W.; Ree, M. *Adv. Mater.* **2005**, *17*, 696.
4. Lee, B.; Park, Y. H.; Hwang, Y. T.; Oh, W.; Yoon, J.; Ree, M. *Nature Materials* **2005**, *4*, 147.
5. Rottman, C.; Grader, G.; DeHazan, Y.; Melchior, S.; Avnir, D. *J. Am. Chem. Soc.* **1999**, *121*, 8533.
6. Dantas de Morais, T.; Chaput, F.; Bailot, J. P.; Lahlil, K.; Darracq, B.; Levy, Y. *Adv. Mater.* **1999**, *11*, 107.
7. Lev, O.; Tsionsky, M.; Rabinovich, L.; Glezer, V.; Sampath, S.; Pankratov, I.; Gun, J. *Anal. Chem.* **1995**, *67*, 22.
8. Harmer, M. A.; Farneth, W. E.; Sun, Q. *J. Am. Chem. Soc.* **1996**, *118*, 7708.
9. Smaihi, M.; Jermoumi, T.; Marignan, J.; Noble, R. D. *J. Membr. Sci.* **1996**, *116*, 211.
10. Huang, E.; Toney, M. F.; Volksen, W.; Mecerreyes, D.; Brock, P.; Kim, H. C.; Hawker, C. J.; Hedrick, J. L.; Lee, V. Y.; Magbitang, T.; Miller, R. D. *Appl. Phys. Lett.* **2002**, *81*, 2232.
11. Lee, H. J.; Lin, E. K.; Wang, H.; Wu, W. L.; Chen, W.; Moyer, E. C. *Chem. Mater.* **2002**, *14*, 1845.
12. Bolze, J.; Ree, M.; Yoon, H. S.; Chu, S. H.; Char, K. *Langmuir* **2001**, *17*, 6683.
13. Oh, W.; Hwang, Y. T.; Park, Y. H.; Ree, M.; Chu, S. H.; Char, K.; Lee, J. K.; Kim, S. Y. *Polymer* **2003**, *44*, 2519.
14. Whang, C. M.; Lim, S. S. *Bull. Korean Chem. Soc.* **2000**, *21*, 1181.
15. Parratt, L. G. *Phys. Rev.* **1954**, *95*, 359.
16. Shin, Y. C.; Choi, K. Y.; Jin, M. Y.; Hong, S. K.; Cho, D.; Chang, T.; Ree, M. *Korea Polym. J.* **2001**, *9*, 100.
17. Lee, B.; Yoon, J.; Oh, W.; Hwang, Y.; Heo, K.; Jin, K. S.; Kim, J.; Kim, K. W.; Ree, M. *Macromolecules* **2005**, *38*, 3395.
18. Gibaud, A.; Vignaud, G.; Sinha, S. K. *Acta Crystallogr.* **1993**, *A49*, 642.
19. Kiessig, H. *Annln. Phys.* **1931**, *10*, 769.
20. Yoon, J.; Heo, K.; Oh, W.; Jin, K. S.; Jin, S.; Kim, J.; Kim, K. W.; Chang, T.; Ree, M. *Nanotechnology* **2006**, *17*, 3490.
21. Oh, W.; Hwang, Y.; Shin, T. J.; Lee, B.; Kim, J.-S.; Yoon, J.; Brennan, S.; Mehta, A.; Ree, M. *J. Appl. Cryst.* **2007**, *40*, s626.